Towards understanding myometrial regulation: metabolomic investigation reveals new pathways of oxytocin and ritodrine activity on the myometrium

Enitome E. Bafor, PhD[1,2*], Edward G. Rowan, PhD[1], RuAngelie Edrada-Ebel, PhD[1*]

[1]*Strathclyde Institute of Pharmacy and Biomedical Sciences, University of Strathclyde, Glasgow, United Kingdom*

This work was supported by the Educational Trust Fund, Nigeria to Dr. Enitome E. Bafor

*Correspondence to: Dr. Enitome E. Bafor and Dr. RuAngelie Edrada-Ebel E-mail: enitome.bafor@uniben.edu; and ruangelie.edrada-ebel@strath.ac.uk respectively

[2]Present address: Department of Pharmacology & Toxicology, Faculty of Pharmacy, University of Benin, Edo State Nigeria.

ABSTRACT

In recent times, additional pathways involved in myometrial regulation and also in the action of oxytocin and β-adrenergic agonists on the myometrium, other than what has been known previously has been suggested. Knowledge of other pathways will prove useful in designing better therapies for myometrial pathologies. This study was therefore aimed at investigating the possibility of other pathways involved in the activity of either oxytocin or a β-adrenergic agonists (ritodrine was used in this study) in myometrial activity with the aid of metabolomics and bioinformatics. High resolution Fourier transform mass spectrometry (HRFTMS), and nuclear magnetic resonance (NMR) spectroscopy coupled with functional uterine assays were combined for an innovative assessment. In vitro pharmacological assay of oxytocin (1 nM) and ritodrine (0.1 nM) on isolated mice uteri mounted in 3 ml organ baths were performed. Mice uteri, treated with oxytocin (OT) or ritodrine (RIT), as well as the physiological buffer in which the uterine tissues were immersed, were rapidly collected and analysed using HRFTMS, ^{1}HNMR and bioinformatics. Resulting data were analyzed via pair-wise chemometric comparison models with $p \leq 0.05$ considered statistically significant. In addition to previously known metabolites, anandamide, nicotinamide adenine dinucleotide, gamma aminobutyric acid and sphingosine were significantly associated with OT's activity while a downstream involvement of prostaglandin F_1 and phosphatidylinositol signalling was observed with RIT's activity. These findings adds evidence to the reports on additional regulation of myometrial activity by these drugs and also offers newer pathways for therapeutic manipulation.

Keywords: Uterus; Oxytocin; Ritodrine; pharmacology; metabolomics

Introduction

The uterus has been described as 'the poor sister among isolated tissues in the pharmacologist's armamentarium' because it is difficult to work with[1]. This difficulty has created gaps in our current understanding of uterine function and associated pathologies (e.g. preterm birth). Comprehensive studies on uterine metabolite profiling appear to be sparse. The need for increased comprehension of myometrial metabolites perturbed during uterine contraction stimulation and/or inhibition is therefore essential for the development of effective treatments and early diagnosis of myometrial pathologies in a bid to counter prevailing reproductive health issues. The important roles played by metabolites in smooth muscle cells cannot be overemphasized. The use of new techniques such as metabolomics shows great potential in improving current knowledge on uterine functioning and has therefore been employed in this study

Oxytocin (OT) is a known uterine contraction stimulant and ritodrine (RIT) a β-adrenergic agonist is a known uterine relaxant, however some molecular and cellular mechanisms underlying oxytocin-induced modulation of uterine contractility are not completely understood [2]. OT is one of the most potent uterotonic agents known and its effect on uterine contractility is of major clinical importance. It is known that OT generates inositol 1,4,5-trisphosphate (IP_3) and diacylglycerol (DAG) [3] by binding to its cell surface transmembrane receptor (OTR).[4] Through a cascade of activity, IP_3 and DAG metabolites independently mediate the release of Ca^{2+} from intracellular stores and promotes myometrial contraction.[5] This pathway is considered the major pathway that mediates OTR signal after binding with OT and for a long time was considered the only pathway.[5] However, in recent times reports on new pathways involved in OT activity on the myometrium are emerging [6]. For instance, it was recently reported that OTR activates mitogen-activated protein kinase (MAPK) and the Rho kinase pathways

resulting in increased cytosolic phospholipase A_2 and subsequently increased prostaglandin production via the cyclooxygenase (COX) pathway.[7,8] The COX pathway specifically COX-2 is also upregulated by MAPK.[8,9] On the other hand, RIT, via $ß_2$-adrenoceptor activation, is known to activate adenosine triphosphate activated potassium (K_{ATP}) channels and large conductance potassium (BKCa) channels in the myometrium through cyclic adenosine monophosphate (cAMP)-dependent phosphorylation and/or directly via guanosine triphosphate (GTP) metabolite.[10] This pathway is considered the major pathway of RIT in myometrial contraction inhibition. RIT is occasionally used clinically for myometrial relaxation in preterm labour.[11,12]

Metabolites are functional units released within cells in response to signals. Measurement of these metabolites therefore can provide an understanding into the basic mechanisms of several metabolic actions [13]. The key technologies in metabolomics include high resolution Fourier transform mass spectrometry (HRFTMS) and 1D/2D-nuclear magnetic resonance (NMR). These technologies enable the detection and identification of several spectral features employed in mapping out potentially significant metabolites responsible for a number of biological activities [14,15]. Sampling during metabolomic analysis measurement can include biofluids and/or tissues and in such instances the tissue samples can be used to investigate specific information related to the tissue or organ while the study of biofluids projects the metabolic changes that have occurred in an animal's organs [16]. Incorporating metabolomic analysis therefore will further aid in the determination of other pathways involved in the activity of RIT or OT on the myometrium. The innovative use of metabolomics coupled with pharmacological assay has never been applied previously. As a proof of principle however, Shah and colleagues (2009) identified a number of proteins (desmoplakin

isoform 1, stratifin and thrombospondin 1) as potential preterm birth protein biomarkers from cervical vaginal fluids [17].

In this study, we report the use of pharmacology coupled with metabolomic methods for the characterization of mouse myometrial metabolite alterations that have occurred in response to OT and RIT. This study also attempts to identify additional pathways involved in myometrial regulation that can be manipulated for therapeutic purposes.

Materials and methods

All experiments were carried out in accordance with the Animal Health and Welfare (Scotland) Act 2006 and the Public Health Service Policy on Humane Care and Use of Laboratory Animals 2002.

Animals

Female virgin C57BL/6 strain laboratory mice weighing between 19-25 g were employed in this study and obtained from the Biological Procedures Unit of the University of Strathclyde, U.K. Mice were maintained in a controlled environment with temperatures maintained at 25°C and the room conditioned to 60% relative humidity. Mice were also maintained under a 12/12h cycle of light and dark and had free access to food and water. Mice in pro-oestrus and oestrus states were selected via microscopic smear examination and macroscopic (visual) examination for these experiments. Selected animals were euthanized under rising concentration of CO_2 and exsanguinated before excision of the uterine tissues was performed. A total of four animals were employed for each set of experiments.

Contractility Experiments

The dissected uteri were cut into segments of approximately 0.5-0.8 cm in longitudinal length, cleaned of extra connective tissues to provide four preparations per mouse. The segments were then weighed and subsequently mounted in warmed (37 °C) 3 ml organ baths containing normal Krebs-Henseleit physiological solution which was composed of; 118.4 NaCl, 25 $NaHCO_3$, 11.1 Glucose, 4.69 KCl, 2.41 $MgSO_4$, 1.18 KH_2PO_4, 2.5 $CaCl_2$ (mM) and continuously gassed with carbogen (95% O_2, 5% CO_2). Tissues were loaded with an initial tension of 1 g and equilibrated for 30 min before subsequent run of experiments. The differential force and frequency of spontaneous contractions in the longitudinal muscle layer were recorded through Grass (FTO3) isometric force transducers connected via Quad Bridge modules to a PowerLab 4/20 data acquisition system using Chart 3.3 software (AD Instruments, UK) which was used to store and analyze acquired data.

Concentration-Response Studies

A uterine contractile agent (OT) and relaxant (RIT) of known mechanisms of action were used in this study. OT (1 nM), and RIT (0.1 nM) were added to the bath containing uterine tissues. Single concentrations of OT and RIT were added to the bath for 10 min following stable rhythmic spontaneous contractions. Without washing, the uterine tissues were collected at the peak of activity and immediately flash frozen in liquid nitrogen. Flash freezing was achieved by rapidly lifting the tissues out of the organ bath and cutting the threads holding the uterine segments to the transducer and tissue holder. The tissues were then placed into cryovials, immediately capped and immersed into liquid nitrogen the whole procedure lasting approximately 30 sec. Fast

and efficient flash freezing is important as it has been reported that cells/tissues remain responsive to their surrounding until physiologic measures are effected to prevent responses completely [19]. The buffer (3 ml) was similarly collected placed into pre-weighed vials and flash frozen. All samples were subsequently stored at -80°C prior to further experiments.

Metabolite Extraction

Materials for Metabolite Extraction

Deuterated dimethyl sulphoxide (DMSO-d_6) and chloroform ($CDCl_3$), HPLC grade methanol, HPLC grade dichloromethane, OT, carbachol, RIT, verapamil, potassium chloride, dimethyl sulphoxide (DMSO) were purchased from Sigma (U.K.). All drugs were prepared as stock solutions in distilled water, except for RIT which was dissolved in DMSO.

Tissue metabolite extraction

Each flash frozen tissue was homogenized using an ULTRA-TURRAX T8 homogenizer (IKA®- WERKE GmbH & Co., Germany) in 400 µl methanol (MeOH), vortexed for 60 s before being centrifuged using a Force 7 Fisher Scientific UK Limited (Leicestershire, UK) at 13,000 rpm/g for 5 min. The supernatant was collected using a micropipette syringe and formed the polar tissue extracts. The residue was extracted with 400 µl dichloromethane (DCM), vortexed for 60 s and centrifuged at 13,000 rpm/g for 10 mins. The supernatant was also collected and formed the non-polar tissue extracts. Wet homogenization combined with direct extraction has been described as one of the best methods for metabolite extraction from tissues as it gives one of the best

metabolite reproducibility and improves the extraction process [20]. The whole procedure was performed in the cold with the aid of dry ice. The time periods employed were predetermined from preliminary experiments. The supernatant was collected using a micropipette syringe and dried in pre-weighed vials in preparation for further NMR and MS measurements.

Extraction of metabolites released into the buffer solution (bath fluids)

Buffer samples (bath fluids) were freeze-dried and weighed. The dried samples were reconstituted with 500 µl of MeOH and vortexed for 1 min. The solution of the mixture was pipetted out and centrifuged as previously described. The supernatant was collected and named polar fluid extracts. The residue was reconstituted in 600 µl of DCM and followed procedures as described for the tissues to form the non-polar fluid extracts. Again all procedures were performed in the cold with the aid of dry ice.

MS Data Acquisition

The MeOH extracts (both tissue and fluid) were separately reconstituted with 100% MeOH while the DCM extracts were reconstituted in DCM : MeOH at a ratio of 30:70 determined from preliminary experiments as suitable for dissolving the non-polar extracts obtained in this study. Samples were transferred into auto sampler MS vials containing 200 µl inserts for HPLC-MS analysis. HPLC-High resolution Fourier transform mass spectrometry (HRFTMS) analysis was carried out using a Dionex UltiMate® 3000 HPLC system (Thermo Fisher Scientific Inc, Hemel Hempstead, UK) employing a 75.0 x 3.0 mm C18 column (a silica type 5µm C18 ACE HPLC column

(HiChrom Limited, UK)). The column was eluted with a linear gradient of 90% A (0.1% v/v formic acid in water) and 10% B (0.1% v/v formic acid in acetonitrile) mobile phases with a flow rate of 0.3 µl/min over 0-35 min then 100% B for a further 5-min isocratic elution, and a return to starting conditions at 40 min for re-equilibration for the last 5 min, using up a total of 45 min for the run. MS identification and analysis were carried out using a Thermo Scientific Orbitrap-Exactive (Thermo Fisher Scientific Inc, Hemel Hempstead, UK) with a 10 µl injection volume and the mass spectrometer was operated with UV detection at 254 nm using both positive and negative ion modes. Full scan data were collected from 50 to 2000 m/z (mass to charge ratio) with a scan time of 0.1 s. Capillary and cone voltages were set at 3.5 kV and 35 V, respectively; desolvation and low controlled source temperatures.

HRLC-HRFTMS profiling

The HRLC-HRFTMS metabolic profiles of polar and non-polar OT- and RIT-treated tissues and surrounding bath fluids were analysed before and after drug treatment. The resulting data were then pre-processed and analysis was performed with the online metabolomic analysis program, XCMS. The raw LC-MS data obtained were first sliced into positive and negative ion modes before conversion to mzXML files prior to XCMS processing. Identification of metabolites was performed within XCMS online using METLIN database. During processing, a novel nonlinear retention time alignment process is performed. This is sequentially performed with matched filtration, peak detection, and peak matching.[18] Statistical determination was also performed at $p < 0.05$ for each pairwise comparison of control and drug-treated groups, with $p < 0.01$ considered highly significant.

HRLC-HRFTMS Data Analysis

The XCMS peak areas were extracted and imported into the soft independent method of class analogy (SIMCA) –P (version 13.0, Umetrics AB, Umeå, Sweden) for principal component analysis (PCA) and orthogonal partial least squares – discriminant analysis (OPLS-DA). Statistical analyses based on a pairwise comparison of control and treated groups were also acquired for the different drugs. Differentially regulated metabolites with p-values less than 5% and fold change greater than 150% were considered statistically significant and used for subsequent analyses.[19,20] Prior to OPLS-DA modelling, the data were normalized using column centring and Pareto scaling ($1/\sqrt{SD}$ [SD= standard deviation]) before modelling. [20,21] A default sevenfold cross validation was performed on the OPLS-DA model to check for model over fitting, and this was determined from the diagnostic parameters R^2Y (residual sum of squares of all y-variables) and Q^2Y (an estimate of the predictive ability of the model calculated by cross validation of all y-variables). For visualization and interpretation the OPLS-DA score scatter plots, S plots and loading plots with confidence intervals were used. The jack-knifed loading plot was additionally sorted by size in order to separate up- and down-regulated metabolites at each end of the plots.

Bioinformatic analyses were subsequently performed on resulting data using the Ingenuity Pathway Analysis (IPA) tool (Ingenuity Systems, Redwood City, CA) for the pathways search regulated by the identified metabolites. IPA-Metabolomics is a program within IPA that extracts rich pathway information from metabolomics data. Statistical significance was calculated using Fischer's exact test, $p<0.05$ indicated a statistically significant no-random association. For a given data set, IPA automatically generates the pathways that are related to those metabolites.

^{1}H-NMR Measurements

The dried MeOH extracts obtained from both tissue and fluid extraction processes described previously, were weighed and reconstituted in DMSO (200 µl) vortexed for 30 secs and placed in shigemi NMR tubes (5 mm) or capillary NMR inserts for 1D ^{1}H-NMR measurements while the DCM extracts were weighed and reconstituted in $CDCl_3$ (200 µl) and similarly placed in shigemi NMR tubes. Presaturated ^{1}H-NMR experiments were carried out on a JEOL-LA400 FT-NMR spectrometer system (JEOL Ltd, UK) with an AS400 magnet and for ^{1}H using a Pulse Field Gradient "Autotune" 40TH5AT/FG broadband high sensitivity probe to accept 5 mm tubes. One-dimensional ^{1}H-proton with presaturation of the residual water resonance NMR spectra were obtained using the following parameters; 32k data points, spectral width of 5998.4 Hz, an acquisition time of 2.73 s, a relaxation delay of 3.0 s., and pulse width of 5.47 requiring a 3.85 min total acquisition time.

NMR data pre-processing and analysis

All NMR data sets were pre-processed using Mnova version 8.1. The imported spectra were manually phased, apodized at Gaussian = 1.0, and baseline corrected to Bernstein polynomial order fit (order 3). The spectra were binned between δ 0.5 – 9 ppm at bin value of δ0.04 ppm width. Bins representing the residual water and solvent peaks were removed. The total spectra area was then normalized to a total value of 100. This yielded a total of 163 and 165 contiguous data for the polar and non-polar datasets respectively. The resulting data yielded a 2D matrix (n x d). The resulting data matrix was then exported into SIMCA-P software package (version 13.0, Umetrics AB, Umeå,

Sweden). Mean centring was performed before principal component analysis (PCA) and OPLS-DA was applied to the datasets. The biplot was employed for visualisation and to add further information on the NMR data. The S-line was also employed to provide supporting information on the variables. It is similar to a statistical total correlation spectroscopy (STOCSY) [22] and is particularly suitable for spectroscopy data. A colour scale is also utilized for analysis which provides information about the chemical shifts of the dataset and corresponding metabolites that contribute to the differences among groups. Biplots and S-lines derived from the OPLS-DA models are shown in Supplementary figure 2.

^{1}H-NMR Profiling

Superimposed pair-matched ^{1}H-NMR spectra of control versus treated mouse uterine tissues and respective bath fluids are presented in Supplementary figure 6A-H. The spectral resolution of the one dimensional (1D) spectra and 2D proton correlation spectroscopy combined with reported data from the literature [23–30] enabled the identification and assignment of different metabolites at varying chemical shift ranges. The Fourier induction decays were processed using Mnova v.8.1.

A schematic diagram showing the various processes involved in this study is shown in Figure 1.

Results

Effect of Oxytocin and Ritodrine on Spontaneous Uterine Contractions

OT (1 nM) increased the force and frequency of uterine contractions (Fig. 2A and 3A). RIT (10^{-7} M), however decreased contractility of spontaneously contracting tissues (Fig. 2B and 3B). This process was necessary in order to observe and confirm the effect of the drugs on uterine contraction and to observe the effect at the time of tissue collection.

Metabolomic Analyses

After XCMS processing, 17154 and 9891 variables were acquired for polar (OTTP) and non-polar oxytocin treated tissues (OTTNP), respectively while 21340 and 16934 variables were acquired for polar (OTFP) and non-polar oxytocin treated fluids (OTFNP), respectively. For polar (RITTP) and non-polar (RITTNP) ritodrine-treated tissues, 14149 and 32051 variables were respectively acquired, while 23260 and 26770 variables were acquired for polar (RITFP) and non-polar ritodrine-treated fluids (RITFNP), respectively. These numbers included isotopic and adduct ion peaks.

Pathways common to both OT and RIT were extracted and found to include phosphatidylinositol signalling, niacinamide metabolism, cell signalling, DAG signalling and glycerophospholipid and catecholamine metabolism (Table 1).

The OPLS-DA score plots showed distinct separations between the control and treated in all experimental groups. A summary of the parameters acquired for prediction and separation in the OPLS-DA models are shown in supplementary table 1 and 2. An S-plot, which varies slightly from a scatter plot was obtained and used to extract significant metabolites and to explain the contribution of the variables on the MS data

(Fig. 3). From each of these plots, differentially significant metabolites were extracted using the jack knifed column plots arranged in descending order with fitted confidence intervals. Columns with confidence intervals that did not include 0, were considered significant (Supplementary tables 3A for OT and 3B for RIT).

Metabolomic analysis of OT- treated uterine tissues and bath fluids

Reliable models were derived with OPLS-DA for all OT-treated groups (R^2 = 1.0) and the predictive ability was satisfactory, $Q^2 > 0.4$ in all cases (Supplementary table 1 and 2). The OPLS-DA plots showed distinct separations between all OT groups in this study (Fig. 4 placed near here). Several significantly differential metabolites were detected to be either downregulated (negative sign) or upregulated (positive sign). Of interest were myoinositol (fold change (FC) = 1.980); and DAG (FC = -5.989 and -1.264 in tissues and fluids respectively. Also detected were nicotinic acid adenine dinucleotide phosphate (NADP) (FC = 2.858) and gamma amino butyric acid (GABA) (FC = 5.847 and 2.952 in tissues and fluids respectively; tyrosine (FC = 1.395); sphingosine (FC = 2.213 and 1.678); N-arachidonylamine (AEA) (FC = -5.007); several glycerophospholipids such as phosphatidylcholine (PC) with FC = 2.175 and phosphatidylethanolamine (PE) with FC = -3.937) were also detected on OT-treated myometrium (Supplementary table 3A). These metabolites and corresponding pathways derived from the HRFTMS and ^{1}H-NMR are shown in Fig. 5A-D and 6A respectively. Myoinositol and DAG signalling were also detected through multivariate analysis of ^{1}H-NMR studies (Fig. 5) and biplots (Supplementary figure 2).

Metabolomic analysis of RIT- treated uterine tissues and bath fluids

Reliable predictive models were similarly derived for the OPLSDA for all RIT-treated groups (R^2 = 1.0; Q^2 > 0.4 in most cases) (Supplementary table 1A). The OPLS-DA plots also showed distinct separations between all RIT groups in this study (Fig. 4). Several significant differential metabolites were also detected by HRFTMS. Of interest were myoinositol (fold change (FC) = -13.582); AEA (FC = 2.479) and prostaglandin F_1 (PGF_1) (FC = 17.764). Others included tyrosine (FC = 4.078); PC with FC = 15.263 and PE with FC = 3.265 (Supplementary table 3B). Significant metabolites and corresponding pathways derived from the HRFTMS and ^{1}H-NMR are shown in Fig. 5A-D right panel and 6B respectively. Multivariate analysis using the S-line plots (Fig. 6) and biplots (Supplementary figure 2) of metabolites detected by ^{1}H-NMR studies (Supplementary figure 1A-H) enabled the detection of significantly correlated metabolites and pathways; of interest was adenosine nucleotide (FC= 0.7979) associated with cAMP signalling in RIT treatment.

Bioinformatic analysis of OT-treated uterine tissues

Significant functions associated with OT-treated groups were lipid and carbohydrate metabolism, energy production, nucleic acid metabolism and involvement in reproductive system function (Figure 7 left panel). Major pathways detected were myoinositol and DAG signalling (Fig. 8A-D left panel). Creation of a network of interacting and interrelated metabolites and corresponding pathways showed phosphatidylinositol, phosphatidylglycerol and sphingosine pathways as significantly associated pathways (Fig. 9 left panel). Others included serotonin, nitric oxide (NO) and RhoGDI signalling (Fig. 9 left panel).

Bioinformatic analysis of RIT- treated tissues

Significant functions detected were cell signalling, lipid and carbohydrate metabolism, energy production, nucleic acid/amino acid metabolism and involvement in reproductive system function (Figure 7 right panel). Pathways detected for RIT included myoinositol downregulation, DAG and phosphate signalling as major pathways (Fig. 8A – D right panel). A network of interacting metabolites and pathways showed cAMP-mediated signalling, protein kinase and G-protein receptor signalling to be primarily involved with RIT – induced uterine relaxation (Fig. 9 right panel).

Discussion

The observation in this study that myoinositol and N-arachidonyl amine were among the statistically significant metabolites detected in the OT-treated myometrium, correlates with previously documented activities reported on OT-induced uterine contraction.[31–34] Myoinositol is a glucose derivative that functions in several signalling pathways one of which is the phosphatidylinositol signalling pathway [35] activated by OT in the uterus. Other interesting findings in this study were the detection of NADP, GABA and metabolites involved in pyrimidine/purine biosynthesis as well as metabolites involved in NO synthesis, some of which had not been previously associated with the action of OT on the uterus. OT has been associated with the inhibition of K^+-stimulated release of excitatory amino acids (glutamate, aspartate) in the supraoptic nerve via an indirect action on the terminals [12] but not in the myometrium. In this study, GABA was also found to have been released into the bath fluids in the presence of OT. The role of NADP as an alternative second messenger and an additional intracellular Ca^{2+}store (besides the action of IP_3 on the sarcoplasmic

reticulum during uterine contraction) is emerging.[36] This NADP component is coupled with the neurotransmitter glutamate [37] which was a significant metabolite observed in this study). NADP has also been reported to be linked with OT-induced contraction [1] in addition to cyclic ADP-ribose acting on ryanodine receptors.[10] Another interesting finding was the decreased release of DAG from the tissues into the surrounding bath fluid observed in response to OT treatment. The simultaneous release of DAG in response to OT has been previously reported.[38] However, a study showed that inhibition of DAG release did not significantly suppress OT activity in the pregnant rat myometrium. [38] An implication that multiple mechanisms besides IP_3 and DAG exist in relation to the activity of oT on the myometrium.[3] These observations were similarly supported by the results from the ^{1}H-NMR data from the current study. Another interesting finding was the detection of downregulated N-arachidonyl amine (AEA) with FC equivalent to -2.337, on OT treatment. AEA activates cannabinoid receptors which have been recently found expressed in reproductive tissues.[39] Binding of AEA to its receptors has been associated with the reduction and increase of intracellular cAMP levels, regulation of ion channels and NO generation.[40] AEA has been reported to cause both stimulatory and inhibitory effects on uterine contractility.[41,42] Bioinformatic analysis in this study revealed an association of AEA with lipid metabolism during OT treatment. AEA was found to be both increased in tissues and decreased in the surrounding bath fluids on OT treatment in this study. The lipids sphingosine and kynurenic acid were also detected in this study in association with OT activity. A relationship between OT, sphingosine and the lysophospholipids has been previously described [9] but not in the myometrium.

Several metabolites were generated from the action of RIT on spontaneous uterine activity. Downregulation of prostaglandin E_2 (PGE_2) in the bath fluid was

detected as RIT decreased uterine contractility. Bioinformatic analysis showed the upregulation of adenosine monophosphate (AMP) owing to the presence of pyrophosphates and kinases. A significant decrease in the concentration of myoinositol in comparison to OT treatment was also observed suggesting a reduction in the phosphatidylinositol signalling pathway in the presence of RIT which supports recent studies linking cAMP signalling with phosphatidylinositol.[43,44] Decreased AEA concentration was also detected with RIT treatment. DAG as well as phenylalanine (a precursor of the catecholamines) were significantly reduced in relation to RIT treatment.

On examination of the ^{1}H-NMR spectra of polar RIT- treated tissues and bath fluids, the metabolites lactate, leucine, acetate, GABA and glutamate were consistently observed while the spectra of the non-polar tissue and bath fluids showed the presence of hydroxybutyrate (HB), leucine, lactate, acetate, GABA and adenosine. The detection of adenosine suggests the involvement of cAMP with RIT. These findings on RIT activity were additionally supported by the OPLS-DA S-plots and biplots on both the MS and NMR data which showed separations between RIT treated tissues and controls and RIT-treated bath fluids and controls.

Comparison of the bioninformatic profiles of uterine tissues and surrounding bath fluids

Chemometric and bioinformatic analysis of the HRFTMS data revealed significant biologic functions for each group in this study. In OT-treated tissues and bath fluids; lipid metabolism, carbohydrate metabolism, energy production and small molecule biochemistry were significantly affected; eicosanoid synthesis, incorporation of thymidine, and nucleotide synthesis were also significantly related indicating an

involvement of OT with these pathways. In RIT-treated tissues, cell signalling, lipid metabolism and small molecule biochemistry were significantly and in RIT-treated fluids, carbohydrate metabolism, energy production, small molecule biochemistry and lipid metabolism were significantly affected. Of the significant pathways extracted for OT-treated tissues, TCA cycle, myoinositol biosynthesis, gluconeogenesis and inositol triphosphate biosynthesis were upregulated. While of the significant pathways extracted for RIT-treated tissues, a downregulation of myoinositol biosynthesis, upregulation of GABA receptor signalling, gluconeogenesis, DAG biosynthesis, prostanoid biosynthesis, serotonin synthesis and sphingosine metabolism were observed. In the bath fluids however, an upregulation of creatinine phosphate and ceramide/sphingosine biosynthesis were observed. Overall, consistent pertubation of glycerophospholipid metabolism and lipid metabolism were involved in both relaxation and contraction of the uterus in response to drugs suggesting a role for these glycerophospholipids in the regulation of uterine contraction.

Examination of the bioinformaticcnetworks indicated a strong association of OT with myoinositol, inositol triphosphate and diacylglycerol. The involvement of other pathways such as sphingosine, serotonin and NO were also dominant. Examination of the network indicated a strong association of RIT with a G-protein coupled receptor (possibly related to cAMP release and activation) and protein kinase A while the significant involvement of dopamine and ERK signalling were detected and are suggested to be associated with myometrial ß-adrenoceptor activation.

Conclusion

The detection of phosphatidylinositol and DAG pathways in connection with the activity of OT on the uterus as well as the detection of AMP, adenosine and components

involved in the cAMP pathway in connection with the effect of RIT on the uterus validates the sensitivity of this method in the detection of metabolites associated with drug function. The discovery of the involvement of other metabolites such as sphingosine and AEA with the activity of OT and the association of GABA and AEA with the activity of RIT provides a knowledge-based hypothesis for further research.

Acknowledgements

The authors would like to acknowledge Mr. Ofego Efeturi for his invaluable assistance with computer analysis, Dr. Alex T. Zhang for his assistance in the HRESIMS measurements and Dr. Lynsey MacIntyre for her advice on HRMS data analysis and processing. Supporting data can be found in the supplementary materials.

Authors' Note

Enitome Bafor and RuAngelie Edrada-Ebel shared first coauthorship.

Declaration of Conflicting Interests

The author(s) declare no potential conflicts of interest with respect to the research, authorship, and/or article publication.

Funding

This research was funded by the Educational Trust Fund, Nigeria awarded to Dr. Enitome E. Bafor

Supplemental Material

Supplementary materials are available

References

1. Aley PK, Noh HJ, Gao X, Tica AA, Brailoiu E, Churchill GC. A functional role for nicotinic acid adenine dinucleotide phosphate in oxytocin-mediated contraction of uterine smooth muscle from rat. *J Pharmacol Exp Ther*. 2010;333:726-735. doi:10.1124/jpet.110.165837.

2. Augert G, Exton JH. Insulin and oxytocin effects on phosphoinositide metabolism in adipocytes. *J Biol Chem*. 1988;263:3600-3609.

3. Asala AK, Diab AA, Atia KI, Fatthy MA. Cannabinoid Induced Changes in rat Uterine Contractility. *Zagazig Univ Med J*. 2013;19:154.

4. Vrachnis N, Malamas FM, Sifakis S, Deligeoroglou E, Iliodromiti Z. The oxytocin-oxytocin receptor system and its antagonists as tocolytic agents. *Int J Endocrinol*. 2011;2011. doi:10.1155/2011/350546.

5. Smith R. Parturition. *N Engl J Med*. 2007;356:271-283. doi:10.1056/NEJMra061360.

6. Sanborn BM, Ku CY, Shlykov S, Babich L. Molecular signaling through G-protein-coupled receptors and the control of intracellular calcium in myometrium. *J Soc Gynecol Investig*. 2005;12(7):479-487.

7. Riento K, Ridley AJ. Rocks: multifunctional kinases in cell behaviour. *Nat Rev Mol Cell Biol*. 2003;4:446-456. doi:10.1038/nrm1128.

8. Molnar M, Hertelendy F. Signal transduction in rat myometrial cells: Comparison of the actions of endothelin-1, oxytocin and prostaglandin F(2α). *Eur J Endocrinol*. 1995;133:467-474. doi:10.1530/eje.0.1330467.

9. Soloff MS, Jeng YJ, Copland JA, Strakova Z, Hoare S. Signal pathways mediating oxytocin stimulation of prostaglandin synthesis in select target cells. *Exp Physiol*. 2000;85 Spec No:51S - 58S. doi:10.1111/j.1469-445X.2000.tb00007.x.

10. Barata H, Thompson M, Zielinska W, et al. The Role of Cyclic-ADP-Ribose-Signaling Pathway in Oxytocin-Induced Ca 2+ Transients in Human Myometrium Cells. *Endocrinology*. 2004;145:881-889. doi:10.1210/en.2003-0774.

11. Beckonert O, Keun HC, Ebbels TMD, et al. Metabolic profiling, metabolomic and metabonomic procedures for NMR spectroscopy of urine, plasma, serum and tissue extracts. *Nat Protoc*. 2007;2:2692-2703. doi:10.1038/nprot.2007.376.

12. Breton JD, Veinante P, Uhl-Bronner S, et al. Oxytocin-induced antinociception in the spinal cord is mediated by a subpopulation of glutamatergic neurons in lamina I-II which amplify GABAergic inhibition. *Mol Pain*. 2008;4:19.

13. Lin CY, Wu H, Tjeerdema RS, Viant MR. Evaluation of metabolite extraction strategies from tissue samples using NMR metabolomics. *Metabolomics*. 2007;3:55-67. doi:10.1007/s11306-006-0043-1.

14. Lokhov PG, Arckakov AI. Mass spectrometry methods in metabolomics. *Biomeditsinskaya Khimiya*. 2008;54:497-511. doi:10.1134/S1990750809010016.

15. Tawfike AF, Viegelmann C, Edrada-Ebel R. Metabolomics and dereplication

strategies in natural products. *Methods Mol Biol*. 2013;1055:227-244. doi:10.1007/978-1-62703-577-4-17.

16. Heijne WHM, Kienhuis AS, van Ommen B, Stierum RH, Groten JP. Systems toxicology: applications of toxicogenomics, transcriptomics, proteomics and metabolomics in toxicology. *Expert Rev Proteomics*. 2005;2:767-780. doi:10.1586/14789450.2.5.767.

17. Shah SJ, Yu KH, Sangar V, Parry SI, Blair IA. Identification and quantification of preterm birth biomarkers in human cervicovaginal fluid by liquid chromatography/tandem mass spectrometry. *J Proteome Res*. 2009;8:2407-2417. doi:10.1021/pr8010342.

18. Tautenhahn R, Patti GJ, Rinehart D, Siuzdak G. XCMS online: A web-based platform to process untargeted metabolomic data. *Anal Chem*. 2012;84:5035-5039. doi:10.1021/ac300698c.

19. Ni Y, Su M, Qiu Y, et al. Metabolic profiling using combined GC-MS and LC-MS provides a systems understanding of aristolochic acid-induced nephrotoxicity in rat. *FEBS Lett*. 2007;581(4):707-711. doi:10.1016/j.febslet.2007.01.036.

20. Westerhuis JA, van Velzen EJJ, Hoefsloot HCJ, Smilde AK. Multivariate paired data analysis: Multilevel PLSDA versus OPLSDA. *Metabolomics*. 2010;6:119-128. doi:10.1007/s11306-009-0185-z.

21. Statfolio S, Statfolio S. Pareto Analysis. *Analysis*. 2005:1-6.

22. Cloarec O, Dumas ME, Craig A, et al. Statistical total correlation spectroscopy: An exploratory approach for latent biomarker identification from metabolic 1H NMR data sets. *Anal Chem*. 2005;77:1282-1289. doi:10.1021/ac048630x.

23. Palama TL, Fock I, Choi YH, Verpoorte R, Kodja H. Biological variation of Vanilla planifolia leaf metabolome. *Phytochemistry*. 2010;71:567-573. doi:10.1016/j.phytochem.2009.12.011.

24. Vasskog T, Andersen JH, Hansen E, Svenson J. Characterization and cytotoxicity studies of the rare 21:4 n-7 acid and other polyunsaturated fatty acids from the marine opisthobranch Scaphander lignarius, isolated using bioassay guided fractionation. *Mar Drugs*. 2012;10:2676-2690.

25. Ong ES, Chor CF, Zou L, Ong CN. A multi-analytical approach for metabolomic profiling of zebrafish (Danio rerio) livers. *Mol Biosyst*. 2009;5:288-298. doi:10.1039/b811850g.

26. Reis MG, De Faria AD, Do Amaral MDCE, Marsaioli AJ. Oncidinol - A novel diacylglycerol from Ornithophora radicans Barb. Rodr. (Orchidaceae) floral oil. *Tetrahedron Lett*. 2003;44:8519-8523. doi:10.1016/j.tetlet.2003.09.015.

27. Subramanian A, Joshi BS, Roy AD, Roy R, Gupta V, Dang RS. NMR spectroscopic identification of cholesterol esters, plasmalogen and phenolic glycolipids as fingerprint markers of human intracranial tuberculomas. *NMR Biomed*. 2008;21:272-288. doi:10.1002/nbm.1191.

28. Mazzei P, Piccolo A, Nugnes L, Mascolo M, De Rosa G, Staibano S. Metabolic profile of intact tissue from uterine leiomyomas using high-resolution magic-angle-spinning ^{1}H NMR spectroscopy. *NMR Biomed*. 2010;23:1137-1145. doi:10.1002/nbm.1540.

29. Celik O, Sarac K, Hascalik S, Alkan A, Mizrak B, Yologlu S. Magnetic resonance spectroscopy features of uterine leiomyomas. *Gynecol Obstet Invest*.

2004;58:194-201. doi:10.1159/000080020.

30. Griffin JL. The Cinderella story of metabolic profiling: does metabolomics get to go to the functional genomics ball? *Philos Trans R Soc Lond B Biol Sci*. 2006;361:147-161. doi:10.1098/rstb.2005.1734.

31. Gimpl G. The oxytocin receptor system: structure, function, and regulation. *Physiol Rev*. 2001. http://physrev.physiology.org/content/81/2/629.short\npapers2://publication/uuid/BBDC0403-38FA-42ED-BA8F-DB87B94D5384.

32. Zingg HH, Laporte SA. The oxytocin receptor. *Trends Endocrinol Metab*. 2003;14:222-227. doi:10.1016/S1043-2760(03)00080-8.

33. Nakamura H, Itakuara A, Okamura M, et al. Oxytocin stimulates the translocation of oxytocinase of human vascular endothelial cells via activation of oxytocin receptors. *Endocrinology*. 2000;141:4481-4485. doi:10.1210/en.141.12.4481.

34. Marc S, Leiber D, Harbon S. Carbachol and oxytocin stimulate the generation of inositol phosphates in the guinea pig myometrium. *FEBS Lett*. 1986;201:9-14. doi:10.1016/0014-5793(86)80561-0.

35. Loewus FA, Murthy PPN. myo-Inositol metabolism in plants. *Plant Sci*. 2000;150:1-19. doi:10.1016/S0168-9452(99)00150-8.

36. Noble K, Noble K, Matthew A, et al. A review of recent insights into the role of the sarcoplasmic reticulum and Ca entry in uterine smooth muscle. *Eur J Obstet Gynecol Reprod Biol*. 2009;144 Suppl:S11-S19. doi:10.1016/j.ejogrb.2009.02.010.

37. Guse AH, Lee HC. NAADP: a universal Ca2+ trigger. *Sci Signal*. 2008;1:re10. doi:10.1126/scisignal.144re10.

38. Shmygol A, Gullam J, Blanks A, Thornton S. Multiple mechanisms involved in oxytocin-induced modulation of myometrial contractility. *Acta Pharmacol Sin*. 2006;27(7):827-832. doi:10.1111/j.1745-7254.2006.00393.x.

39. Paria BC, Das SK, Dey SK. The preimplantation mouse embryo is a target for cannabinoid ligand-receptor signaling. *Proc Natl Acad Sci U S A*. 1995;92:9460-9464. doi:10.1073/pnas.92.21.9460.

40. Brighton PJ, McDonald J, Taylor AH, et al. Characterization of anandamide-stimulated cannabinoid receptor signaling in human ULTR myometrial smooth muscle cells. *Mol Endocrinol*. 2009;23:1415-1427. doi:10.1210/me.2009-0097.

41. Dmitrieva N, Berkley KJ. Contrasting effects of WIN 55212-2 on motility of the rat bladder and uterus. *J Neurosci*. 2002;22:7147-7153. doi:20026686.

42. Buxton ILO. Regulation of uterine function: a biochemical conundrum in the regulation of smooth muscle relaxation. *Mol Pharmacol*. 2004;65:1051-1059. doi:10.1124/mol.65.5.1051.

43. Breuiller-Fouche M, Charpigny G, Germain G. Functional genomics of the pregnant uterus: from expectations to reality, a compilation of studies in the myometrium. *BMC Pregnancy Childbirth*. 2007;7 Suppl 1:S4. doi:10.1186/1471-2393-7-S1-S4.

44. Charpigny G, Leroy M-J, Breuiller-Fouché M, et al. *A Functional Genomic Study to Identify Differential Gene Expression in the Preterm and Term Human Myometrium.*; 2003. doi:10.1095/biolreprod.102.013763.

Table 1. Significant pathways and metabolites associated with both OT- and RIT-treated groups

Metabolic Pathway	Metabolite	Adducts	m/z	Rt	Fold Change (FC)			
					Oxytocin (OT)		Ritodrine (RIT)	
					Tissue	Fluid	Tissue	Fluid
hosphatidyl-inositol	Myo-inositol	$[M+H-H_2O]^+$	163.0607	1.75	nd	nd	-	nd
ignalling							13.582	
			163.0608	1.75	nd	1.98	nd	nd
icotine/Nicotinamide	Niacinamide	$[M+H]^+$	123.0554	1.80	2.858	nd	nd	nd
athway			123.0554	1.82	nd	nd	4.691	nd
lycine, serine and	Betaine aldehyde	$[M+H]^+$	102.0915	2.13	nd	nd	1.103	3.191
hreonine pathway			102.0914	2.20	-1.332	3.506	nd	nd
yridine/Valine/leucine	Norleucine	$[M+H-H_2O]^+$	340.2593	7.32	-2.337	-1.700	nd	nd
iosynthesis			340.2593	7.32	nd	nd	nd	-735.82
ell signalling	N-methyl	$[M+Na]^+$	340.2593	7.48	-2.337	-1.700	nd	nd
	arachidonoyl amine		340.2593	7.48	nd	nd	nd	-735.82
ell signalling	DAG (22:5)	$[M+H-2H_2O]^+$	679.5118	8.56	-5.989	-1.264	nd	nd
	DAG isomer		679.5119	12.09	nd	nd	nd	-
								24582.82
ipid metabolism	2-keto palmitic acid	$[M+NH_4]^+$	288.2531	17.63	nd	-82.668	nd	-
			288.2531	17.72	nd	nd	nd	-172.505
phingolipid metabolic	Sphingosine	$[M+H]^+$	300.2897	19.03	2.213	1.678	nd	nd
athway	Sphingosine isomer		300.2897	21.31	nd	nd	2.525	nd

Glycerophospho-lipid	PC(18:2(2E,4E)/0:0)	$[M+H]^+$	520.3403	19.40	nd	-	nd	nd
Metabolic pathway						252.938		
			520.3403	19.51	nd	nd	nd	-451.904
Glycerophospho-lipid	PC(O-14:0/2:0)	$[M+H]^+$	496.3401	20.34	2.261	nd	nd	nd
Metabolism			496.3400	20.34	nd	nd	2.108	nd
Glycerophospho-lipid	Glycerophospho-N-	$[M+H]^+$	480.3089	20.96	2.318	nd	nd	nd
Metabolism	oleoyl ethanolamine		480.3087	21.00	nd	nd	2.422	nd
Glycerophospho-lipid	PC(O-	$[M+H]^+$	522.3559	21.71	2.150	nd	nd	nd
Metabolism	16:1(11Z)/2:0)							
			522.3558	21.72	nd	nd	nd	-55.707
Diacylglycerol	1-hexadecyl	$[M+ACN+H]^+$	438.2981	21.76	nd	nd	3.027	nd
Biosynthesis	Lysophosphatidic		438.2981	21.78	2.867	-2.749	nd	nd
	acid							
Glycerophospholipid	PE(18:0/0:0)	$[M+H]^+$	482.3243	24.84	nd	nd	2.175	nd
Metabolic pathway			482.3244	24.86	2.037	nd	nd	nd
Glycerophospho-lipid	PC(P-15:0/0:0)	$[M+H]^+$	466.3294	26.01	3.037	-1.427	nd	nd
Metabolic pathway			466.3294	26.10	nd	nd	2.880	nd
Diacylglcerol	1-Octadecyl	$[M+ACN+H]^+$	466.3294	26.01	3.037	-1.427	nd	nd
Biosynthesis	Lysophosphatidic		466.3294	26.10	nd	nd	2.880	nd
	acid							
Steroid biosynthesis	Dihydroxyvitamin	$[M+H]^+$	545.3850	26.22	nd	-4.637	nd	nd
	D3							
			545.3851	26.67	nd	nd	nd	-34.181
Lipid metabolism/ cell	Oleamide	$[M+H]^+$	282.2791	29.31	2.691	2.085	nd	nd
signalling			282.2791	29.54	nd	nd	5.242	nd

Catecholamine	N-Adenyl-L-	$[M+ACN+H]^+$	536.1659	34.52	nd	-3.606	nd	nd
biosynthesis	phenylalanine		536.1659	35.04	nd	nd	nd	-15508.4

DAG =diacylglycerol,; PC= phosphatidylcholine; PE= phosphoethanolamine; PS= phosphoserine; PG = phosphoglycerol; TG=triacylglycerol; m/z = mass to charge; Rt = Retention time; FC = fold change; PV = p value. A positive FC value indicates a relatively higher metabolite concentration in the treated groups, while a negative value is indicative of a relatively lower concentration in the treated groups.

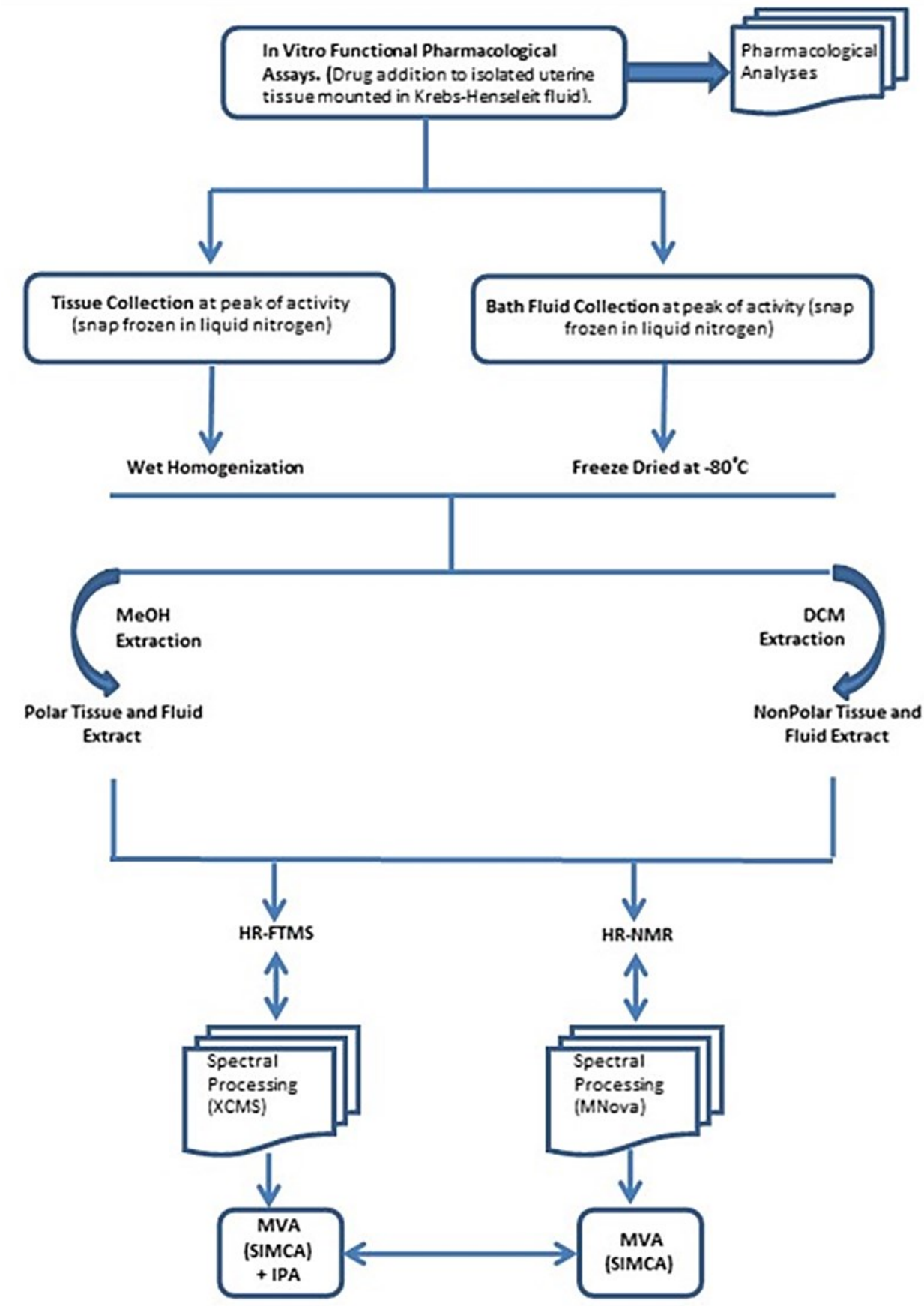
In Vitro Functional Pharmacological Assays. (Drug addition to isolated uterine tissue mounted in Krebs-Henseleit fluid).
Pharmacological Analyses
Tissue Collection at peak of activity (snap frozen in liquid nitrogen)
Bath Fluid Collection at peak of activity (snap frozen in liquid nitrogen)
Wet Homogenization
Freeze Dried at -80°C
MeOH Extraction
DCM Extraction
Polar Tissue and Fluid Extract
NonPolar Tissue and Fluid Extract
HR-FTMS
HR-NMR
Spectral Processing (XCMS)
Spectral Processing (MNova)
MVA (SIMCA) + IPA
MVA (SIMCA)

Figure 1. Flow chart showing the steps involved in the study.

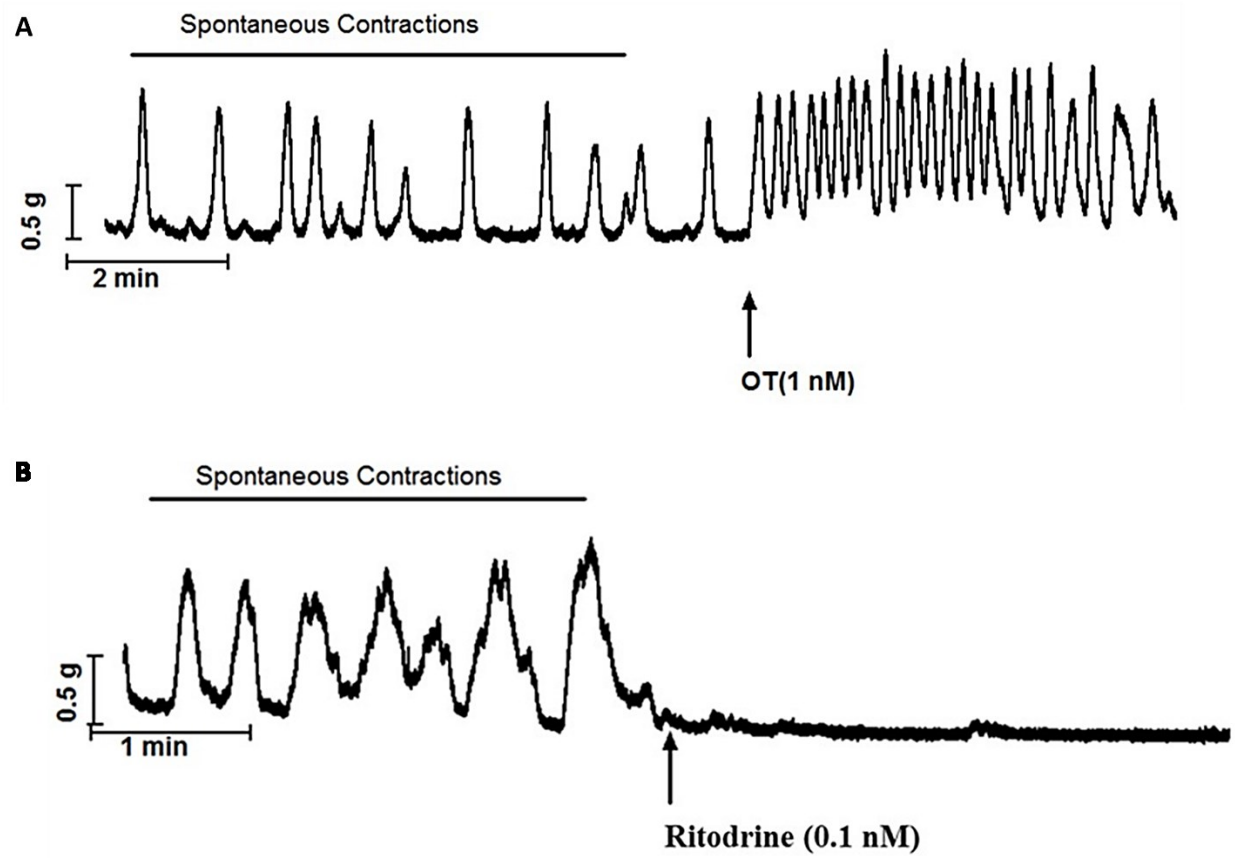

Figure 2. Representative recordings of the effect of OT (1 nM) (A) and ritodrine RIT (0.1 nM) (B) on spontaneously contracting mouse uterine tissues

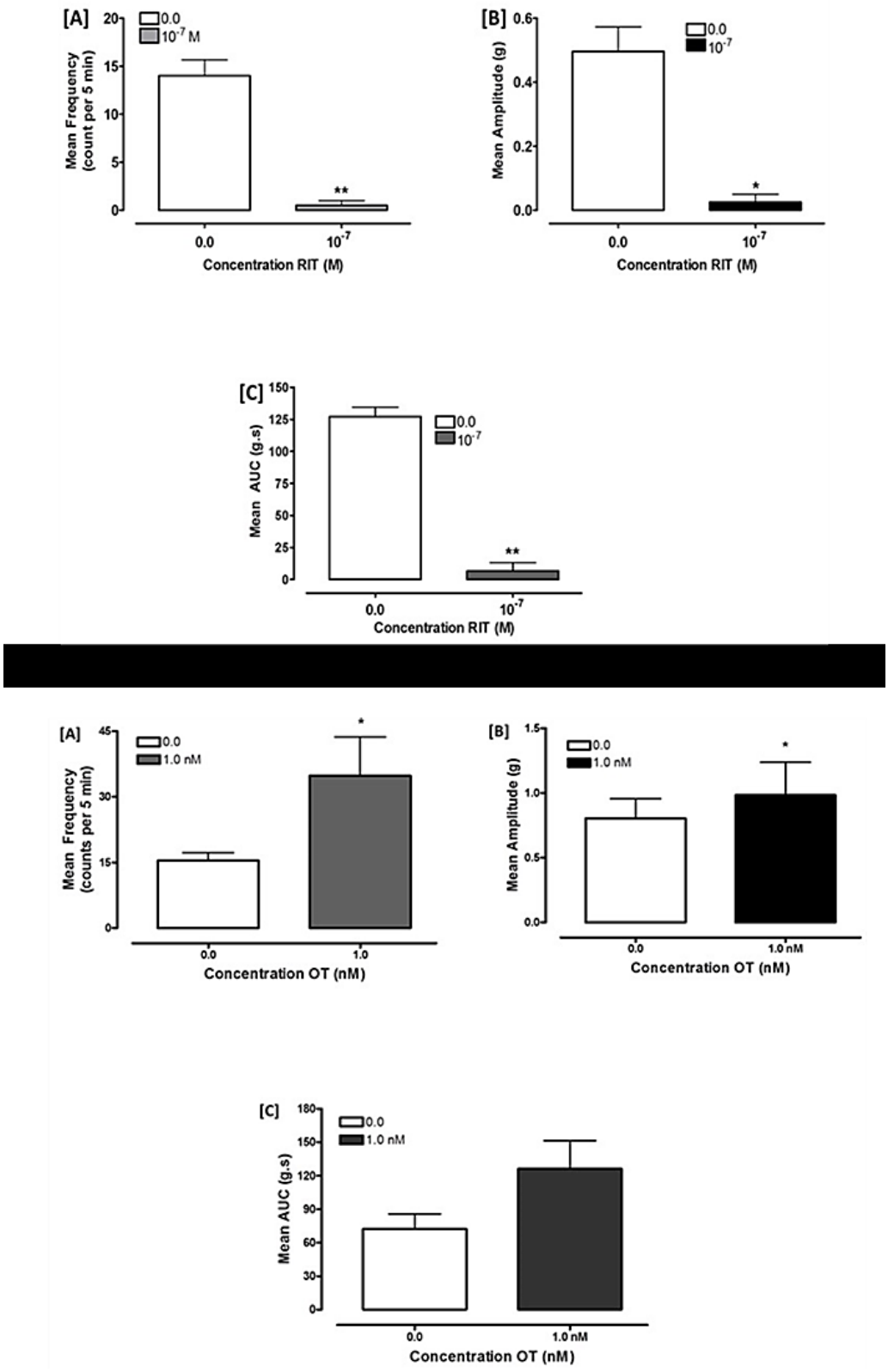

Figure 3. Mean responses (± S.E.M) of the isolated uterus to OT (bottom panel) and RIT (top panel) calculated within a 5 min time range. In each panel, (A) Frequency; (B) Amplitude of uterine contractions, and (C) the area under the curve. Spontaneous

contractions which occurred in the absence of drug were considered as the control (0.0). Experiments were performed at 37˚C. * = $p<0.05$ compared with the control (analysed using the t-test). n = 5 animals.

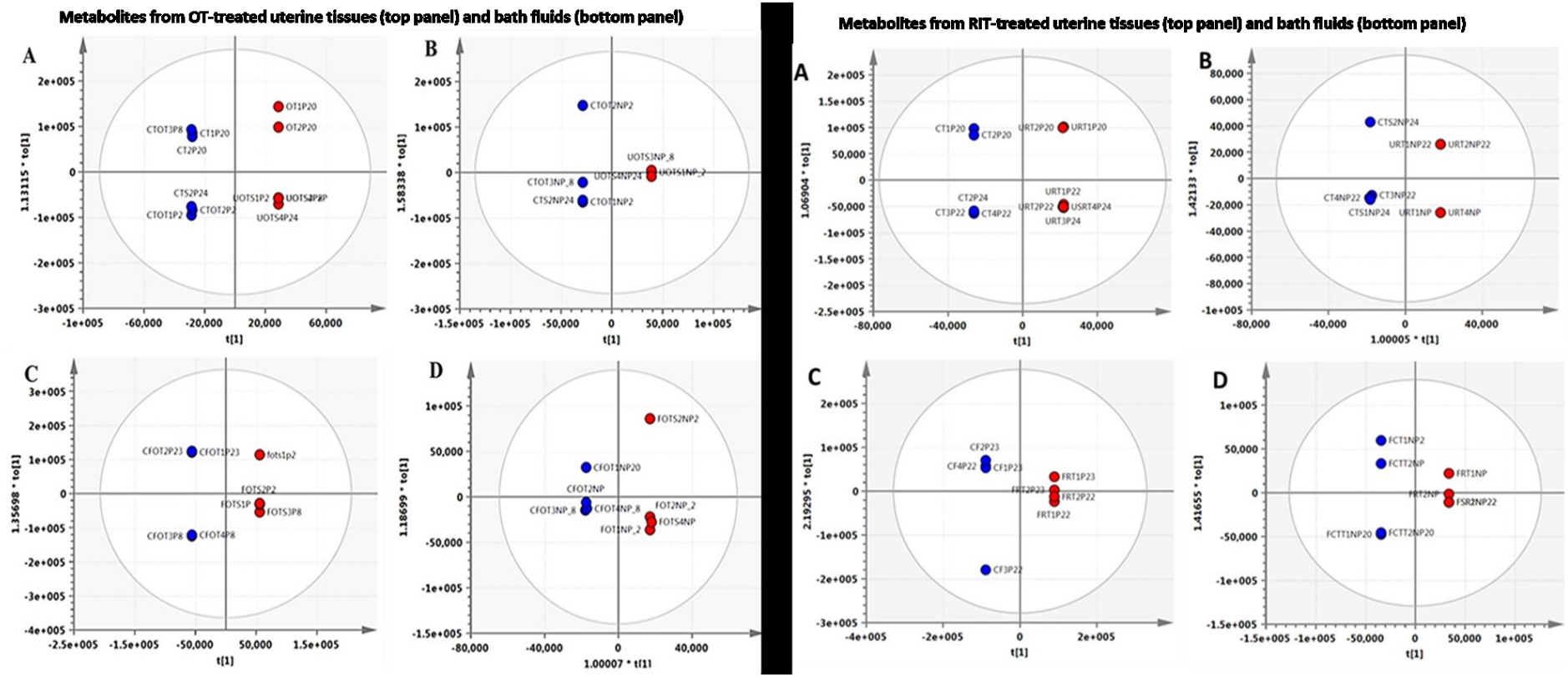

Figure 4 OPLS-DA scatter score plots of differentially synthesized metabolites observed on treatment of the isolated uterus with OT (left panel)and RIT (right panel) as determined by HRFTMS. The red circles represent the treated groups while the blue circles represent the controls. n = 5 animals

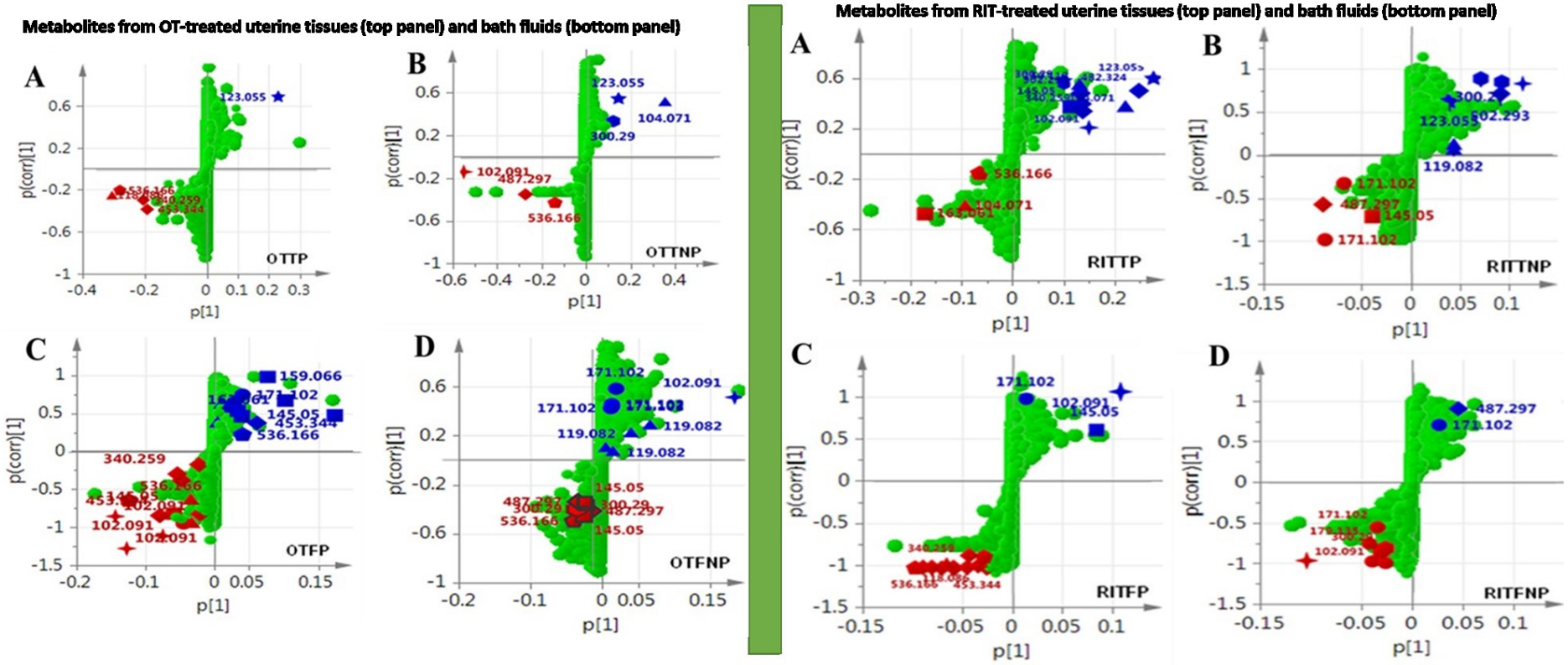

Figure 5 S-Plots of differential regulated metabolites with OT (left panel) and RIT (right panel) treatment of the isolated uterine tissues (A-B) and the surrounding bath fluid (C-D) as determined by HRFTMS. The green circles represent all metabolites detected for the particular group. Significantly regulated metabolites in the control groups are highlighted in blue shapes while those in the treated groups are highlighted in red shapes with corresponding m/z values**. OTTP** = OT-treated polar tissues; **OTTNP** = OT-treated non-polar tissues; **OTFP** = OT-treated polar

bath fluids; **OTFNP** = OT-treated non-polar bath fluids. **RITTP** = RIT-treated polar tissues; **RITTNP** = RIT-treated nonpolar tissues; **RITFP** = RIT-treated polar bath fluids; **RITFNP** = RIT-treated nonpolar bath fluids. □□ Signal Transduction (PGF1□)□ □ □ Phosphatidyl-inositol signalling system; ▲ = Ligand-receptor Interaction/Lipid Metabolism(GABA); □ □ cAMP biosynthesis; □ □ Sphingolipid metabolism; □ = Cell Signalling (Arachidonic acid); □ = Nicotine/Nicotinamide metabolism; □ = Glycine, serine and threonine metabolism. The key metabolites that were perturbed are listed in Table 1. n = 5 animals

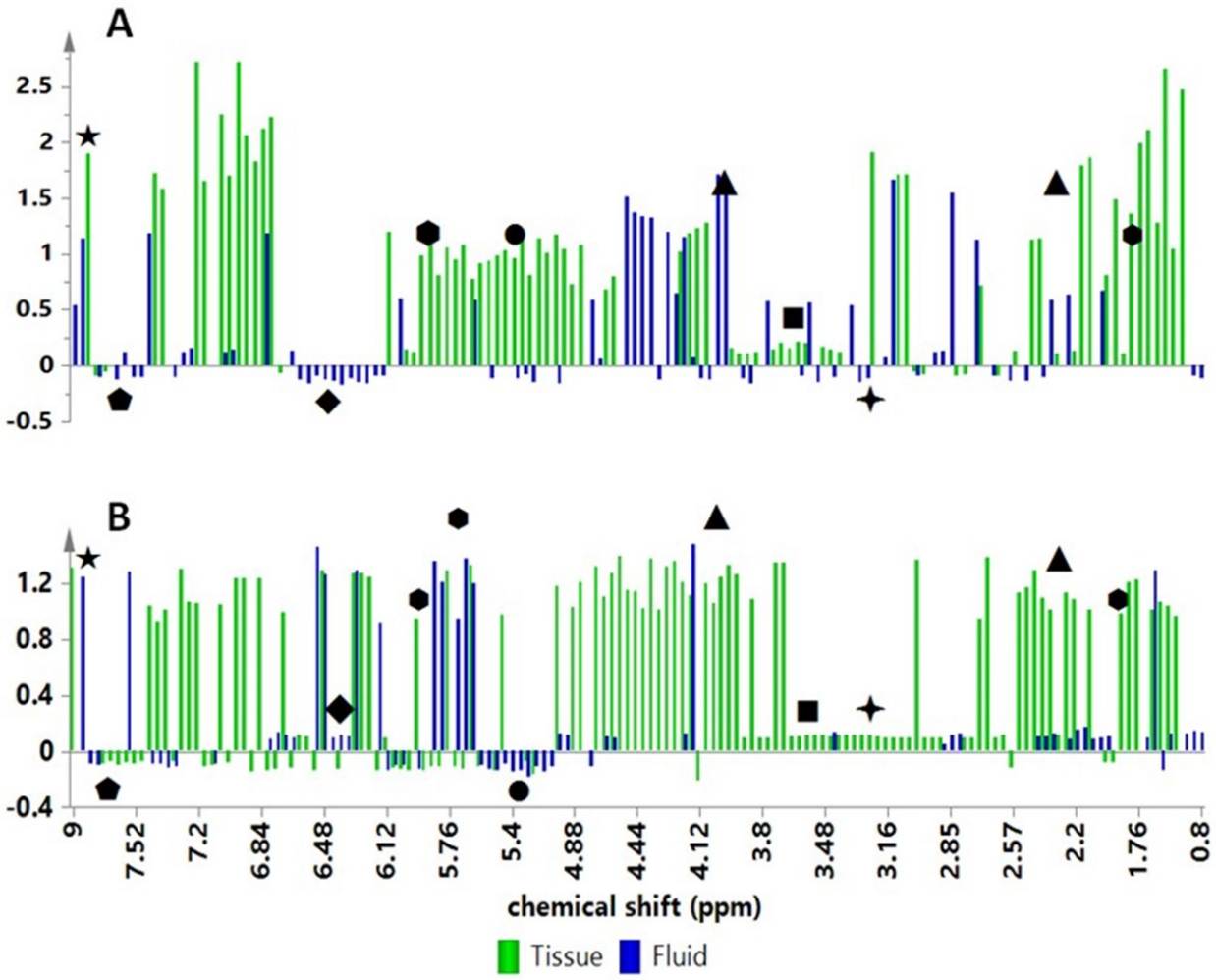

Figure 6 Differentially regulated metabolites with OT (A) and RIT (B) as determined by

NMR**.** A positive p[1] value indicates a relatively higher metabolite concentration in the treated groups, while a negative value is indicative of a relatively lower concentration in the treated□ □= Signal Transduction (PGF1□)□ □= Phosphatidyl-inositol signalling system (myoinositol); ▲ = Ligand-receptor Interaction/Lipid Metabolism (GABA/DAG); □ = cAMP biosynthesis (N-Adenylyl-L-phenylalanine); □ = Sphingolipid metabolism; □= Cell Signalling (Arachidonic acid); □ = Nicotine/Nicotinamide metabolism; □ = Glycine, serine and threonine metabolism (betaine). n= 5 animals

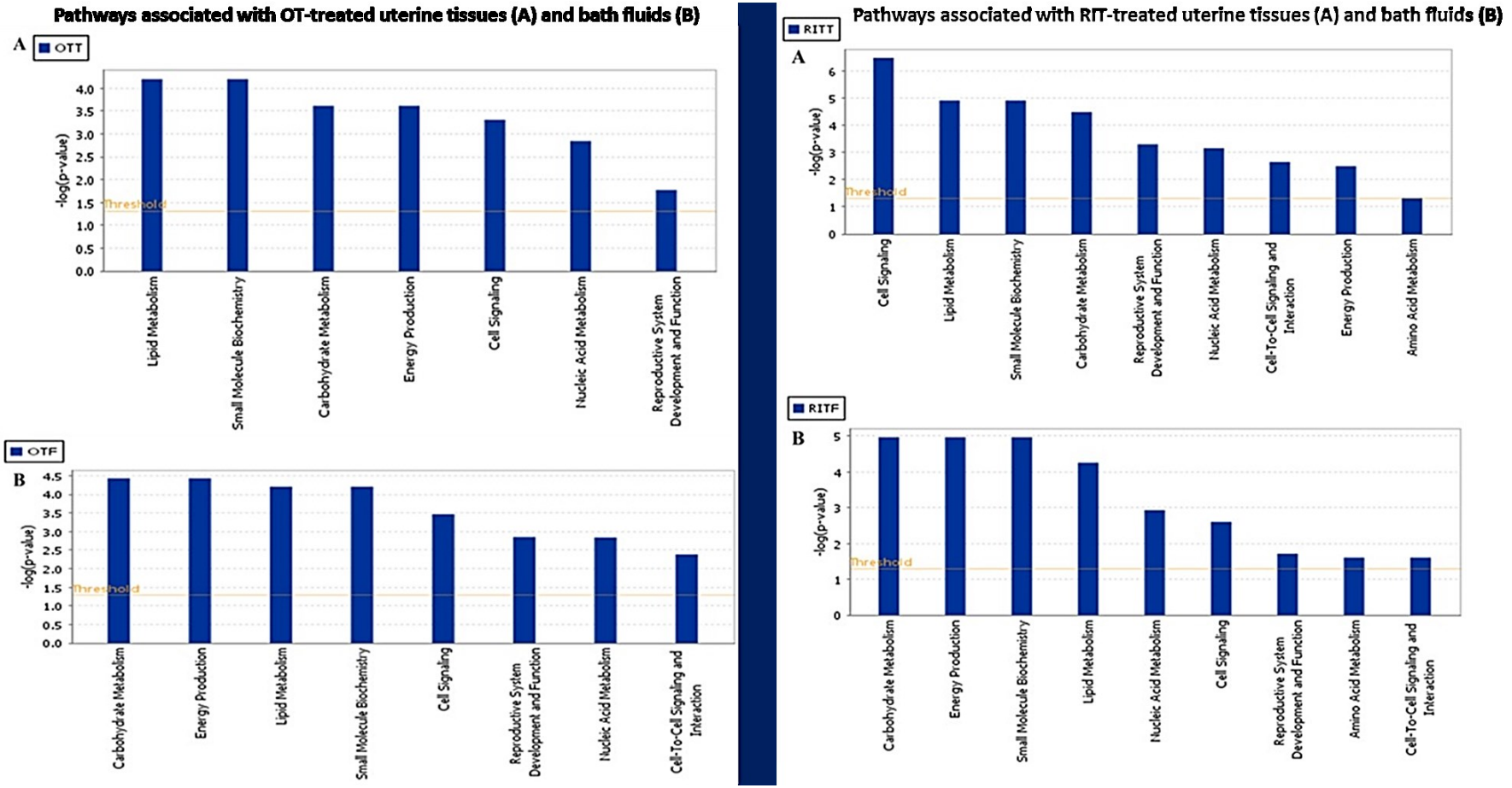

Figure 7 Top functions extracted by IPA software that have been perturbed on treatment of the isolated uterus with oxytocin (left panel) and RITTT (right panel). Functions associated with OT- and RIT- treated tissues and fluids are shown in A and B above along the x-axis while the –

log (p-value) is indicated on the left y-axis. Taller bars are more significant than shorter bars. The orange line is indicative of the cut-off for significance $p<0.05$ (-log = 1.3). n = 5 animals

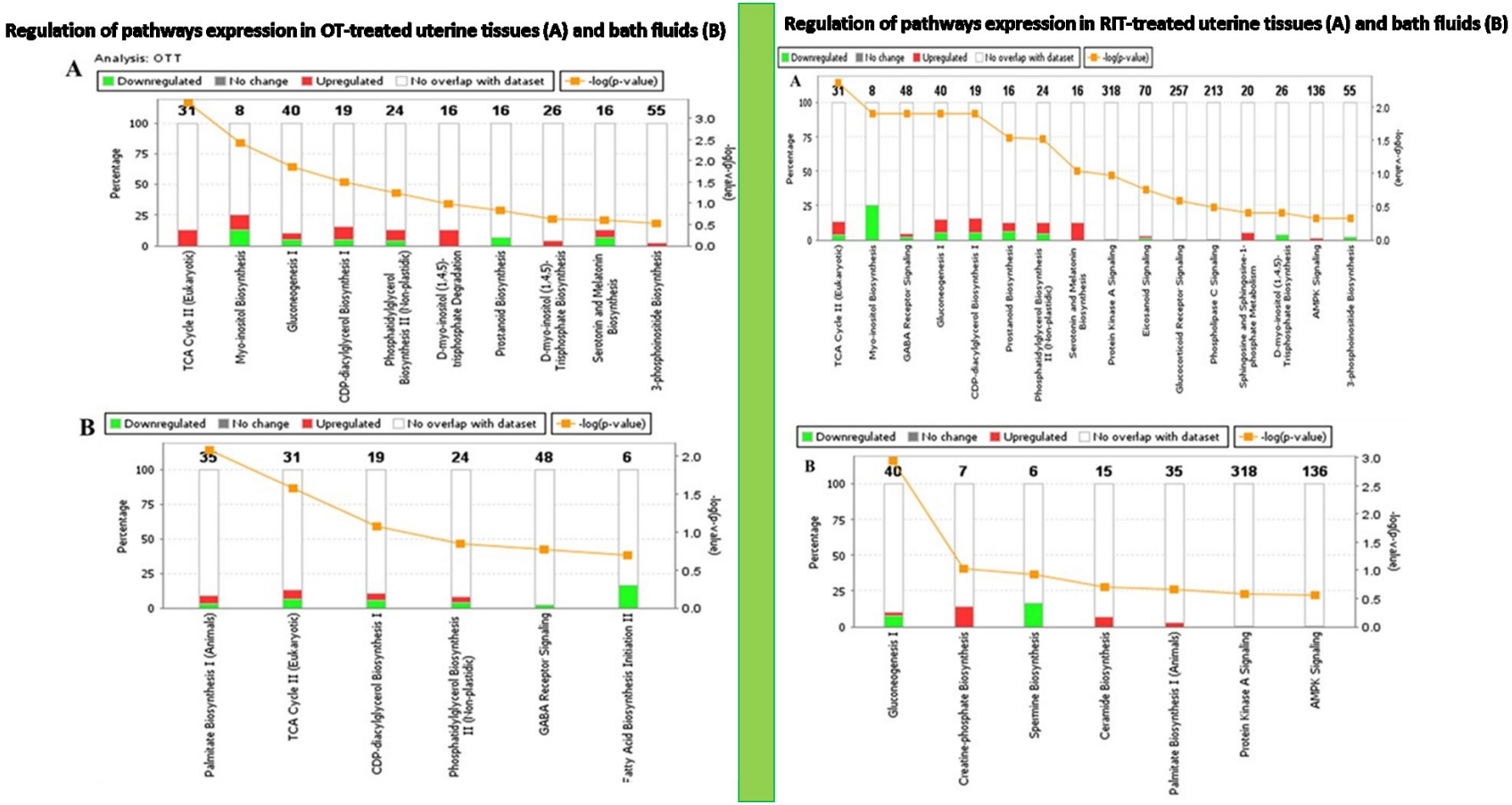

Figure 8 Top canonical pathways for OT (left panel) and RIT (right panel) extracted by IPA bioinformatics software. Pathways associated with OT-treated uterine tissues are shown in A while the bath fluids are shown in B. The pathways are displayed along the x-axis. The stacked bar charts represent the overlap of the analysis with the canonical pathways. The green bars represent downregulation and the red bars represent upregulation. The orange line is indicative of the cut-off for significance $p<0.05$. n = 5 animals

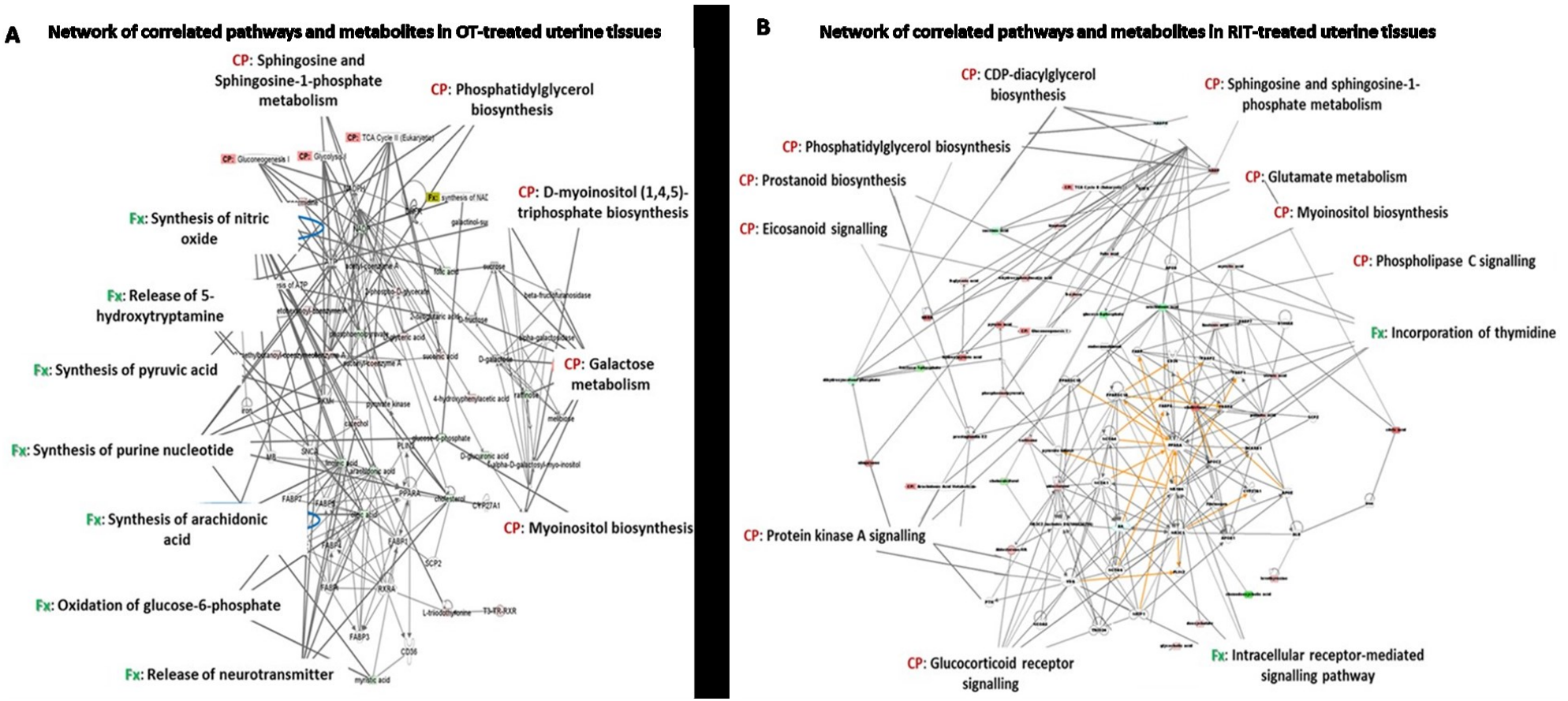
A
Network of correlated pathways and metabolites in OT-treated uterine tissues
CP: Sphingosine and Sphingosine-1-phosphate metabolism
CP: Phosphatidylglycerol biosynthesis
CP: D-myoinositol (1,4,5)-triphosphate biosynthesis
Fx: Synthesis of nitric oxide
Fx: Release of 5-hydroxytryptamine
Fx: Synthesis of pyruvic acid
CP: Galactose metabolism
Fx: Synthesis of purine nucleotide
Fx: Synthesis of arachidonic acid
CP: Myoinositol biosynthesis
Fx: Oxidation of glucose-6-phosphate
Fx: Release of neurotransmitter
B
Network of correlated pathways and metabolites in RIT-treated uterine tissues
CP: CDP-diacylglycerol biosynthesis
CP: Sphingosine and sphingosine-1-phosphate metabolism
CP: Phosphatidylglycerol biosynthesis
CP: Prostanoid biosynthesis
CP: Glutamate metabolism
CP: Myoinositol biosynthesis
CP: Eicosanoid signalling
CP: Phospholipase C signalling
Fx: Incorporation of thymidine
CP: Protein kinase A signalling
CP: Glucocorticoid receptor signalling
Fx: Intracellular receptor-mediated signalling pathway

Figure 9 IPA network of top functions and signalling pathways detected on analysis of OT- (left panel) and RIT- (right panel) treated uterine tissues. The network displays the interaction and interrelationship between the metabolites detected on drug treatment. The interconnectivities were then pulled together into specific biological functions and pathways. FX = function; CP= canonical pathways.